

Joint Correction of Ionosphere Noise and Orbital Error in L-Band SAR Interferometry of Interseismic Deformation in Southern California

Zhen Liu, Hyung-Sup Jung, *Member, IEEE*, and Zhong Lu, *Senior Member, IEEE*

Abstract—The accuracy of L-band synthetic aperture radar (SAR) differential interferometry (InSAR) on crustal deformation studies is largely compromised by ionosphere path delays on the radar signals. The ionosphere effects cause severe ionospheric distortion such as azimuth streaking and long wavelength phase distortion similar to orbital ramp error. Effective detection and correction of ionospheric phase distortion from L-band InSAR images are necessary to measure and accurately interpret surface displacement. In this paper, we investigate the performance improvement of L-band InSAR interseismic deformation measurements in southern California through the joint correction of both ionosphere noise and orbital error. Our results show that this method can effectively remove orbit and ionosphere phase distortions. In comparison with *in situ* GPS measurements, the achieved InSAR measurement accuracy is improved from ~ 30 mm to ~ 10 mm by the proposed joint correction method. We show that, after the joint correction, the remaining atmosphere noise can be further mitigated through stacking, leading to an RMS error of ~ 4.7 mm/year in resultant line-of-sight velocity, as compared with ~ 11.3 mm/year before the correction. Our results demonstrate that the proposed joint correction technique provides a promising way to jointly correct orbital and ionospheric artifacts in L-band InSAR studies of crustal deformation.

Index Terms—ALOS PALSAR, interferometric SAR (InSAR), ionospheric correction, ionosphere noise, multiple-aperture interferometry (MAI), orbital error, synthetic aperture radar (SAR).

I. INTRODUCTION

SATELLITE synthetic aperture radar (SAR) differential interferometry (InSAR) is now a widely used technique

Manuscript received March 27, 2013; revised June 17, 2013; accepted July 1, 2013. This work was supported in part by the Jet Propulsion Laboratory, California Institute of Technology under a contract with the National Aeronautics and Space Administration and in part by the The University of Seoul under financial support from Space Core Technology Development Program through the National Research Foundation of Korea funded by the Ministry of Education, Science and Technology under Grant 2012M1A3A3A02033465 and State-of-the-Art Remote Sensing Technology Development of Disaster Management Research Program funded by the National Disaster Management Institute under Grant NDMI-M-2012-09.

Z. Liu is with the Jet Propulsion Laboratory, California Institute of Technology, Pasadena, CA 91109 USA (e-mail: Zhen.liu@jpl.nasa.gov).

H.-S. Jung is with the Department of Geoinformatics, The University of Seoul, Seoul 130-743, Korea (e-mail: hsjung@uos.ac.kr).

Z. Lu is with the U.S. Geological Survey, Cascades Volcano Observatory, Vancouver, WA 98683-9589 USA (e-mail: lu@usgs.gov).

Color versions of one or more of the figures in this paper are available online at <http://ieeexplore.ieee.org>.

Digital Object Identifier 10.1109/TGRS.2013.2272791

for measuring relative surface displacements along the radar line-of-sight (LOS) direction between SAR acquisitions with accuracy of an approximately millimeter to centimeter level at a fine spatial resolution (~ 100 m or higher) over a large area [1]–[3]. The success and accuracy of this technique in measuring surface deformation are strongly affected by various noise sources inherent in InSAR measurements. These typically include orbital error, troposphere artifact, ionosphere phase delay, residual topography error, and decorrelation noise. For an L-band SAR system, one dominant noise source is the ionosphere effect due to the propagation of the SAR wave through the ionosphere. The ionosphere's frequency-dependent refractive index leads to wave dispersion, inducing phase delays on radar pulses that are directly proportional to the total electron content (TEC) and inversely proportional to the radar frequency [4] and [5]. Ionosphere phase delay causes significant interferometric phase errors, including small-scale phase distortions due to ionosphere turbulence and long-wavelength phase artifacts that are similar to orbital error. The spatial and temporal variability of TEC associated with solar activity also cause heterogeneous effects of the propagation delay on a SAR image and result in considerable spatiotemporal interferometric phase variations [6].

The ionospheric influence on SAR, InSAR, and polarimetric SAR has been recently studied [4], [6], [7]. A number of approaches for the ionosphere correction have been proposed [4]. These approaches either exploit the ionosphere effect from the range and/or azimuth spectrum of single SAR image or interferogram, or study the ionosphere effect on polarization through Faraday rotation [7]. To correct ionospheric effects on InSAR phase imagery, several methods have been proposed, including the range split-spectrum method [8]–[10], the range group-phase delay difference method [4], [8], [9], and the azimuth shift method that is based on the relationship between the azimuth derivative of the ionospheric effect and the azimuth displacement [4] and [5].

Recently, Jung *et al.* [11] have examined these different methods and have proposed an improved azimuth shift method to estimate the TEC variation between SAR acquisitions and ionosphere phase distortion. This new method utilizes an improved multiple-aperture interferometry (MAI) technique [12]–[14] to construct a multiaperture interferogram. It then exploits the linear relationship between the MAI phase and the azimuth

derivative of the ionospheric phase to estimate the TEC variation and ionosphere-induced interferometric phase shift. A test on a limited data set shows that the method can remove the ionosphere phase distortion successfully. Further analysis also demonstrates that the improved method can estimate TEC variation with accuracy better than $\sim 10^{-4}$ TEC units at 100 or more multilooking level and 0.5 coherence level, which is significantly better than other azimuth shift methods [11]. Because the method of [11] uses MAI [12] and [15] rather than the pixel offset from cross correlation of two SAR amplitude images [5] to estimate the interferometric phase due to azimuth displacement, it improves the accuracy of the measurement.

In this paper, we investigate the improvement of L-band InSAR interseismic deformation measurements from joint corrections of the ionosphere noise and orbital error. The measurements are from two Advanced Land Observation Satellite (ALOS) Phase Array L-band SAR (PALSAR) L-band InSAR pairs that cover the southern San Andreas-San Jacinto fault system. Both InSAR images are subject to severe ionosphere phase distortion with long wavelength features similar to deformation signals and orbital ramp errors. We show that the joint correction method allows the effective removal of large ionosphere and orbital artifacts. We also show that, after the joint correction, it is possible to further reduce remaining noise components such as atmosphere delay by resorting to conventional methods such as stacking or temporal filtering in InSAR time-series analysis.

II. METHOD

In the following, we describe the joint correction method of ionospheric noise and orbital error, including a brief description of the MAI-based ionosphere correction method for phase distortion. More details about the MAI-based ionosphere correction method can be referred to [11].

The ionosphere correction method exploits the linear relationship between the MAI phase and the azimuth gradient of ionosphere phase, which can be expressed as

$$\frac{\partial \phi_{\text{ion}}}{\partial x} = -\alpha \cdot \frac{l}{n\lambda} \cdot \phi_{\text{MAI}} \quad (1)$$

where ϕ_{MAI} is the MAI phase, x is the azimuth, $\partial \phi_{\text{ion}} / \partial x$ is the azimuth derivative of the ionospheric phase, α is a system- and geometry-dependent factor, l is the effective antenna length, λ is the radar wavelength, and n is a normalized squint that is a fraction of the full aperture width. Consequently, the ionospheric phase can be expressed by the integration of the MAI phase extending from A to B as $\phi_{\text{ion}} = -\alpha \cdot l / n\lambda \cdot \int_A^B \phi_{\text{MAI}} dx$. Furthermore, according to [11], the relationship between the InSAR phase and the MAI phase exists as

$$\frac{\Delta \phi_{\text{InSAR}}(x, r)}{\Delta_{\text{az}}} = \alpha \cdot \bar{\phi}_{\text{MAI}}(x, r) + \beta \quad (2)$$

$$\Delta \phi_{\text{InSAR}}(x, r) = \phi_{\text{InSAR}}(x + 1, r) - \phi_{\text{InSAR}}(x, r) \quad (3)$$

where Δ_{az} is multilooked azimuth pixel spacing, r is the range, and β is the offset value used to calculate the reference phase of the MAI interferogram. $\bar{\phi}_{\text{MAI}}(x, r)$ is the scaled MAI phase and defined as $\bar{\phi}_{\text{MAI}}(x, r) = -(l/n\lambda)\phi_{\text{MAI}}(x, r)$. $\Delta \phi_{\text{InSAR}} / \Delta_{\text{az}}$

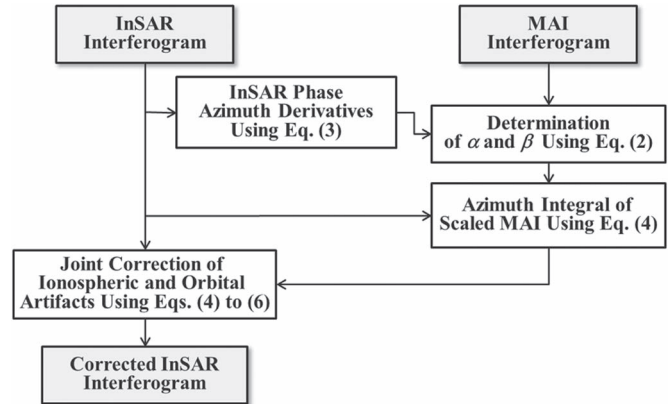


Fig. 1. Processing flow summarizing major steps in the joint correction of ionospheric and orbital errors.

is the azimuth derivative of InSAR phase, and $\Delta \phi_{\text{InSAR}}(x, r)$ is the InSAR phase difference along the azimuth. Once parameters of α and β are estimated using linear regression, the ionospheric phase ϕ_{ion} can be calculated as

$$\phi_{\text{ion}}(x, r) = \sum_{u=1}^x [(\alpha \cdot \bar{\phi}_{\text{MAI}}(u, r) + \beta) \cdot \Delta_{\text{az}}] + C(r) \quad (4)$$

where $C(r)$ is the integral constant that varies along the range direction. The integral constants can be estimated using the correlation between ionospheric and InSAR phase [11] and [16].

Jung *et al.* [12] found that the residual flat earth and topographic phase in MAI interferograms are approximate functions of the perpendicular baseline difference between forward- and backward-looking pairs, and the flat earth phase is generally much larger than the topographic phase. They also showed that a second-order polynomial model could be used to remove such phase distortions. However, the model does not work well for MAI interferograms that have severe ionosphere distortion since the ionosphere phase is much larger than the flat earth phase in the MAI interferograms. Thus, the insufficient correction of the MAI phase distortions could cause a nonlinear phase distortion in the ionospheric phase ϕ_{ion} calculated from the azimuth integration in (4). This phase distortion is more severe in azimuth direction and can be approximately modeled by a second-order polynomial in both azimuth and range directions. Note that, when the flat earth phase is very small, such phase distortion due to insufficient correction of the flat earth phase is negligible.

A polynomial fitting method has been used for the removal of the phase distortion induced by the orbital error, which is frequently adopted in InSAR processing [17]. The orbital phase ϕ_{orb} can be modeled by

$$\phi_{\text{orb}}(x, r) = a_0 + a_1x + a_2r + a_3xr + a_4x^2 + a_5r^2 + a_6h(x, r) \quad (5)$$

where a_0, a_1, \dots and a_6 are the model parameters, and $h(x, r)$ is the topographic height at (x, r) . The $h(x, r)$ can be used for the mitigation of topography-dependent atmospheric artifact. If the spatial extent of the deformation signal is much

TABLE I
CHARACTERISTICS OF ALOS PALSAR PAIRS USED IN THIS STUDY

Master	Slave	Beam Mode	Incidence Angle (deg.)	$f_{DC,f}^b$ (Hz)	$f_{DC,e}^b$ (Hz)	$f_{DC,b}^b$ (Hz)	$\angle f_{D,S}^c$ (Hz)	B_{\perp}^d (m)	$\angle B_{\perp}^d$ (m)
15/07/2007	20/10/2009	FBS ^a	38.7	482.7	79.4	-324.0	792.6	-270.8	-0.028
15/10/2007	20/10/2009	FBS	38.7	474.5	71.1	-332.3	804.0	-890.5	-0.054

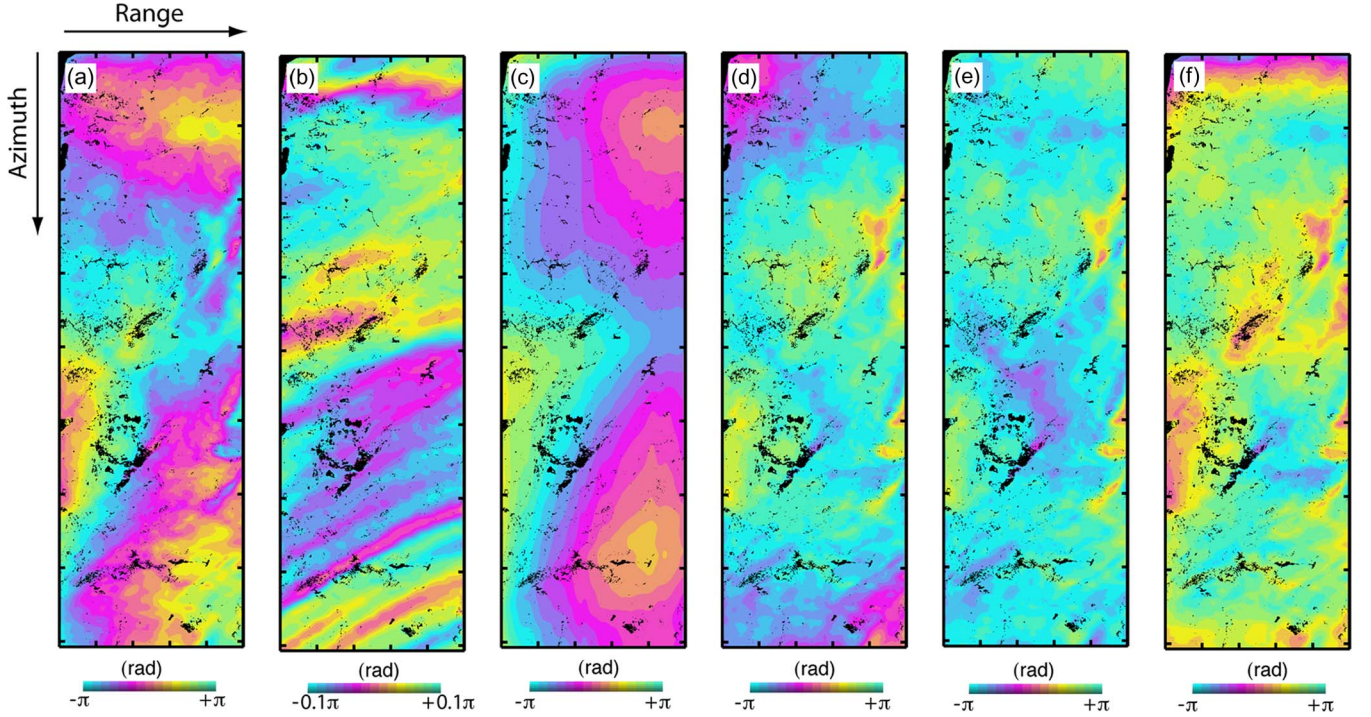


Fig. 2. (a) Original InSAR interferogram. (b) MAI interferogram. (c) Ionospheric phase map estimated from the MAI interferogram. (d) ionosphere-corrected InSAR interferogram after MAI-based ionosphere phase correction. (e) Jointly corrected InSAR interferogram after joint correction of ionosphere and orbit error. (f) Orbit-corrected InSAR interferogram after orbital phase estimation from 2-D polynomial fit of the original InSAR interferogram. All interferograms and phase map are for the pair of 2007/07/15–2009/10/20. The area of low coherence is masked. Note that one fringe in the MAI interferogram represents 0.2π .

smaller than the orbital error, the orbital ramp parameters can be determined by a fitting to the interferometric phase of all coherent pixels.

Finally, the corrected interferometric phase $\hat{\phi}_{\text{InSAR}}$ can be defined as

$$\hat{\phi}_{\text{InSAR}}(x, r) = \phi_{\text{InSAR}}(x, r) - \phi_{\text{ion}}(x, r) - \phi_{\text{orb}}(x, r). \quad (6)$$

From (4) and (5), we can estimate the phase distortions caused by ionosphere noise and orbital error. We, then, remove them from InSAR phase using (6). Since the ionospheric phase may possess nonlinear phase distortions due to insufficient correction of the residual flat earth phase in azimuth and range directions that can be modeled as a second-order polynomial function similar to the orbital phase model in (5), the orbital phase correction should be applied after the MAI-based ionosphere phase correction.

The processing flow of the method is summarized in Fig. 1. Major steps include the following: 1) estimate and generate the InSAR phase azimuth derivative map from the unwrapped InSAR interferogram using (3); 2) determine the parameters of α and β from the InSAR phase azimuth derivative map and

the unwrapped scaled MAI interferogram using (2); 3) generate the ionospheric phase map from the azimuth integral of the scaled MAI interferogram using (4); and 4) generate a corrected InSAR interferogram from the joint correction of ionospheric and orbital artifacts by subtracting orbital error map estimated from (5) after subtracting the ionospheric phase map from the InSAR interferogram.

Note that, in the presence of long-wavelength deformation signals, the orbital error estimated from the polynomial fitting method may include long wavelength components of the deformation signal. We need to further correct the overcorrection by using *in situ* GPS measurements as control points, leading to the separation of two dominant long wavelength noise sources from imaged deformation signals. It needs to be mentioned that the MAI-based ionosphere phase correction method will not be needed if the azimuth displacements due to ionosphere contribution can be negligible or if the pattern of the ionospheric phase map is similar to that of the orbit error phase map. Moreover, we need to carefully handle the MAI-based ionosphere phase correction method if the azimuth displacements due to ground deformation are not negligible.

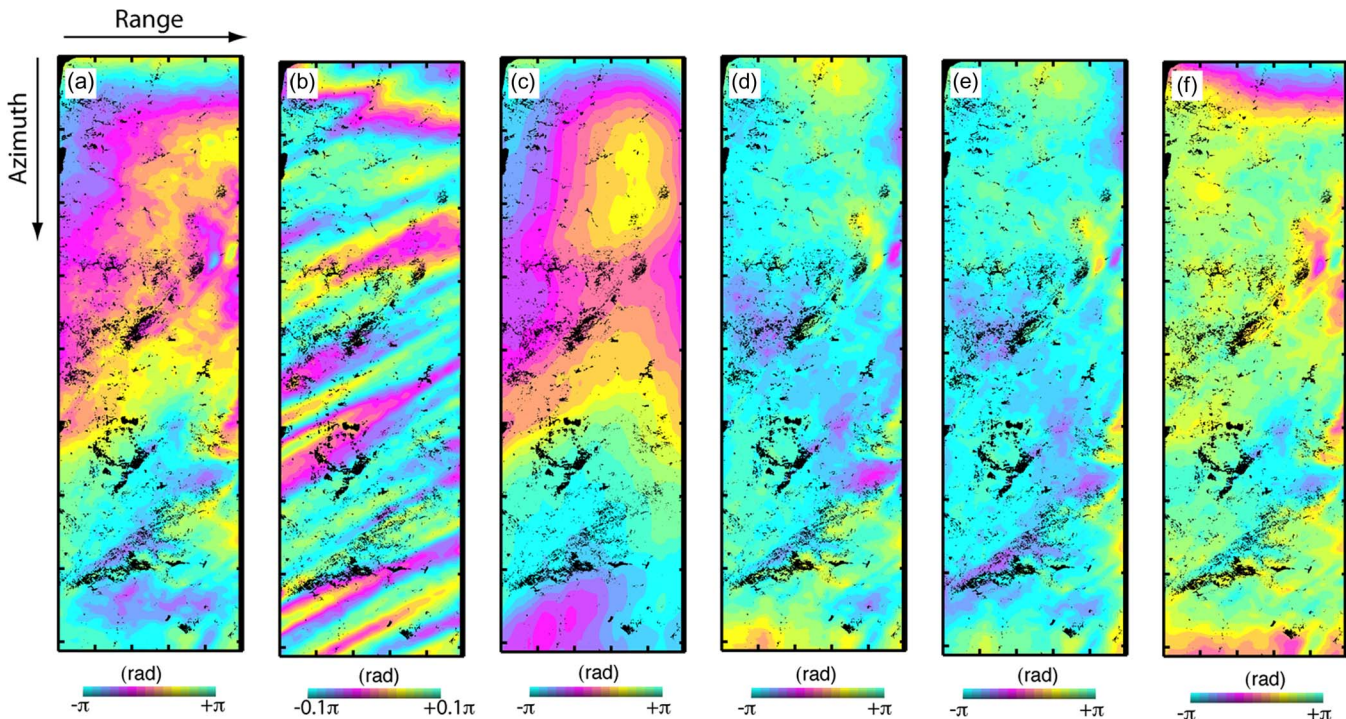


Fig. 3. (a)–(f) are the same as Fig. 2 but for the pair of 2007/10/15–2009/10/20. The area of low coherence is masked. Note that one fringe in the MAI interferogram represents 0.2π .

III. RESULTS

We apply our method of joint correction of ionosphere noise and orbital error to two InSAR interferograms in southern California. The raw SAR data are from the Japanese ALOS PALSAR sensor. Four frames (640, 650, 660, 670) from the ascending track 214 are concatenated to generate single-look complex (SLC) SAR scenes and form the interferograms. The InSAR interferograms are multilooked by 5×20 looks in range and azimuth directions, respectively, resulting in roughly $\sim 60 \times 63$ m pixels. The interferograms are smoothed using an adaptive filter [18] with a window size of 64 to reduce phase variance.

The MAI interferograms are generated by an improved MAI approach [12]. A normalized squint of 0.5 and an effective antenna length of 8.9 m, respectively, are used for the MAI processing. For the MAI processing, the forward, average, and backward Doppler centroids and the subaperture processing bandwidth are calculated by azimuth common band filtering and summarized in Table I. The forward- and backward-looking SLC images are first produced from raw radar signal. Forward- and backward-looking interferograms are then generated, multilooked, and smoothed by the same multilooked factor and filter used for the InSAR processing. The final MAI interferograms are generated after the correction of residual flat-earth and topographic phase [12]. Both InSAR and MAI interferograms can be coregistered by simple translation since they have the same relative geometry [11]. We then base on the processing steps summarized in Section II to estimate the ionosphere noise and orbit error of InSAR interferogram.

Fig. 2 shows the original InSAR interferogram (a), MAI interferogram (b), MAI-based estimates of the ionospheric phase map (c), ionosphere-corrected InSAR interferogram

using MAI-based correction (d), InSAR interferogram after the joint correction of ionosphere phase and orbital error (e) and, for comparison purpose, orbit-corrected InSAR interferogram after orbital phase estimation from 2-D polynomial fitting of the original InSAR interferogram, and (f) for the InSAR pair 2007/07/15–2009/10/20. Results for the pair 2007/10/15–2009/10/20 are shown in Fig. 3. It is clear that both pairs are dominated by severe long-wavelength ionospheric phase noise [see Figs. 2(c) and 3(c)]. For example, for the pair 2007/07/15–2009/10/20, phase variations due to the ionosphere phase artifact range from ~ -3.9 to 6.7 rad, corresponding to LOS displacements of ~ -7.3 to ~ 12.6 cm. This is particularly problematic for interseismic deformation mapping since expected deformation signals due to fault slip/locking are small. The maximum variations of the MAI phase are ~ -0.64 to $+0.93$ rad for the pair 2007/07/15–2009/10/20, and $\sim \pm 0.9$ rad for the pair 2007/10/15–2009/10/20. These correspond to the along-track displacements of ~ -0.9 to ~ 1.3 m and $\sim \pm 1.3$ m, respectively, which are much larger than expected azimuthal displacements (< 7 cm) due to interseismic deformation [22]. Moreover, it is also noted that the shape of the ionospheric phase map shown in Figs. 2(c) and 3(c) is deformed to fit into that of the original InSAR interferograms shown in Figs. 2(a) and 3(a). This is because the integration constants of (4) are estimated using the correlation between ionospheric and InSAR phase. We can see that our method of joint correction of ionosphere and orbital errors can successfully estimate and correct the major components of ionosphere and orbital phase distortions [see Figs. 2(e) and 3(e)]. We also find that the 2-D polynomial fitting, which is commonly used for orbital error correction in InSAR processing, appears to remove a large portion of ionospheric and orbital phase signals

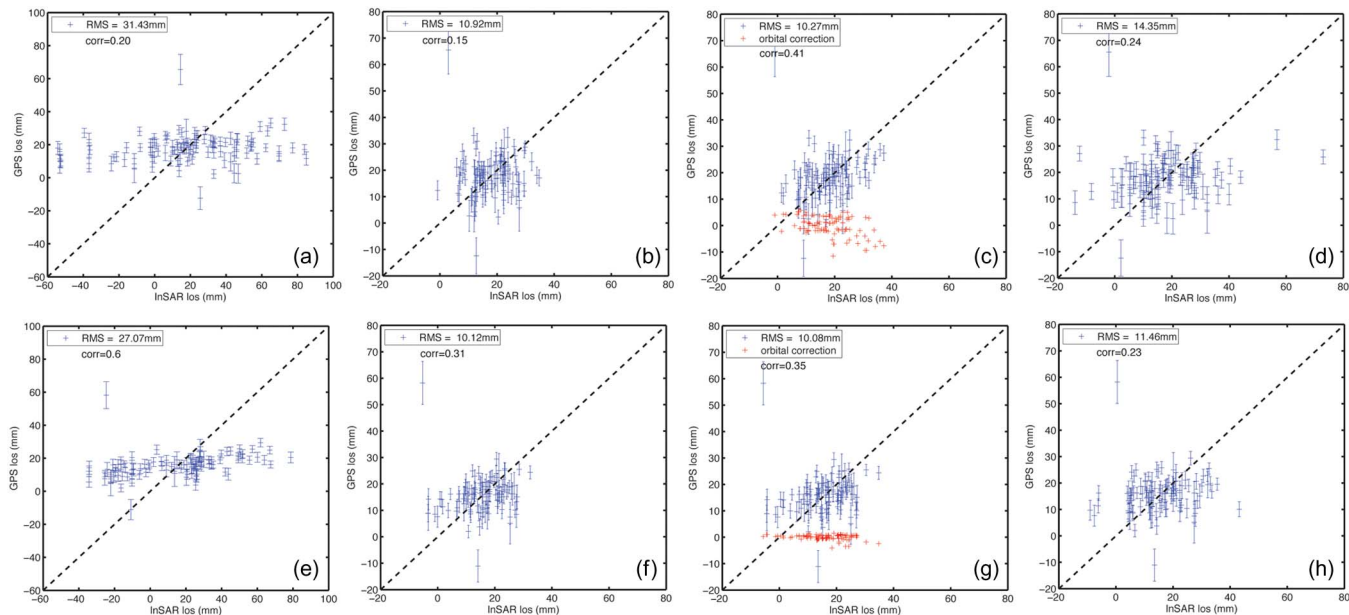


Fig. 4. Projected GPS LOS displacements versus InSAR LOS displacements from (a) and (e) original InSAR interferograms; (b) and (f) ionosphere-corrected interferograms using MAI-based ionosphere phase estimation; (c) and (g) jointly corrected interferograms after correcting both ionospheric phase distortion and orbital ramp error; and (e)–(h) orbit-corrected interferograms using orbital phase estimation from 2-D polynomial fitting. The RMS errors quantify the difference between InSAR and GPS LOS displacements of blue crosses. Error bars denote uncertainties of projected GPS LOS measurements at two standard deviations. (a)–(d) are for the pair of 2007/07/15–2009/10/20. (e)–(h) are for the pair of 2007/10/15–2009/10/20. In (c) and (g), red crosses indicate estimated orbital ramp errors at GPS locations versus corrected InSAR LOS displacements.

because of long-wavelength characteristics of such noises [see Figs. 2(f) and 3(f)]. However, there are considerable amounts of ionospheric phase noises remained, particularly at the beginning and ending parts of each interferogram.

To validate our correction results, we use *in situ* GPS velocities from southern California Earthquake Center (SCEC) Community Motion Map-4 (CMM-4) [19] as the ground truth of interseismic deformation measurements. Fig. 4 shows the comparison between projected GPS and InSAR LOS displacements. The root-mean-square (RMS) error is used to quantify the difference between GPS and InSAR LOS displacements at the same GPS locations indicated in Fig. 6(a). Artificial correlation between InSAR and GPS LOS displacements due to ionosphere phase artifacts exists before the correction [see Fig. 4(a) and (e)]. After the MAI-based ionosphere phase correction, the RMS errors and correlation coefficients are changed from ~ 31.4 mm and 0.20 to ~ 10.9 mm and 0.15 for the pair 2007/07/15–2009/10/20, and ~ 27.1 mm and 0.60 to ~ 10.1 mm and 0.31 for the pair 2007/10/15–2009/10/20 [see Fig. 4(b) and (f)], respectively. These results suggest that the correction successfully removes the dominant ionosphere phase artifact. Note that such MAI-based ionosphere phase correction is not perfect. The ionosphere-corrected InSAR interferograms may still have phase distortions due to the orbital error and/or the undercorrection of the MAI phase distortion. These can be further corrected by the 2-D polynomial fit. Considering the risk of removing deformation signals due to the polynomial fitting, we make further correction by using GPS as ground control points. We perform a 2-D polynomial fit to the difference between corrected InSAR and GPS LOS displacements and remove the ramp error from InSAR data using the best-fit parameters. The resultant RMS errors are ~ 10.3 mm for

the pair 2007/07/15–2009/10/20 and ~ 10.1 mm for the pair 2007/10/15–2009/10/20 [see Fig. 4(c) and (g)], respectively. Joint correction of the orbital error improves the RMS error but only marginally, suggesting that orbital ramp errors from both pairs are small. In comparison, the orbital and ionospheric phase corrections based on 2-D polynomial fit do not achieve the same level of RMS error reduction as the joint correction method [see Fig. 4(d) and (h)]. There is much larger scattering between InSAR and GPS LOS displacements, consistent with what we observe in Figs. 2(d) and 3(d).

After the joint correction of ionosphere noise and orbital ramp error, remaining major noise components in L-band SAR interferometry are mainly atmospheric phase delay, which are random in time and can be further suppressed through some conventional approaches such as stacking [20] or temporal filtering in InSAR time-series analysis [2], [3], [21]. We test this by stacking the derived LOS velocities from two InSAR pairs before and after the joint correction (see Fig. 5). Although the InSAR pairs have the same slave image, their stacking clearly reduces the scattering associated with individual interferograms and improves the RMS error in resultant LOS velocity. The RMS error in LOS rate is reduced from ~ 5.1 mm/year for a single pair after the joint correction to ~ 4.7 mm/year after the stacking. Considering both pairs share the same ending date, atmosphere noise is not completely random. We still achieve an RMS error reduction of $\sim 8\%$ by using just two pairs. Again, we observe much larger scattering in the stacked LOS velocity based on interferograms that are corrected for the orbital and ionospheric phase using a 2-D polynomial fit [see Fig. 5(c)]. Fig. 6 shows the map view of stacked LOS velocity before and after the correction of ionospheric and orbital phase artifacts.

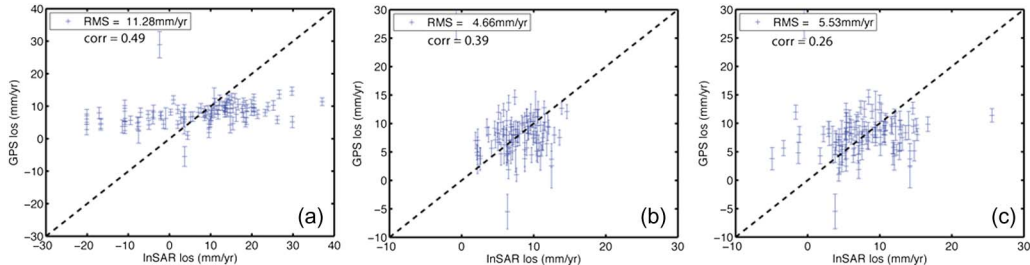


Fig. 5. Projected GPS LOS velocities versus InSAR LOS velocities derived from the stacking of (a) original InSAR interferograms; (b) jointly corrected interferograms after correcting MAI-based ionosphere phase estimation and orbital ramp error; and (c) orbit-corrected interferograms using orbital phase estimation from 2-D polynomial fitting. The RMS errors are used to quantify the difference between InSAR and GPS LOS velocities.

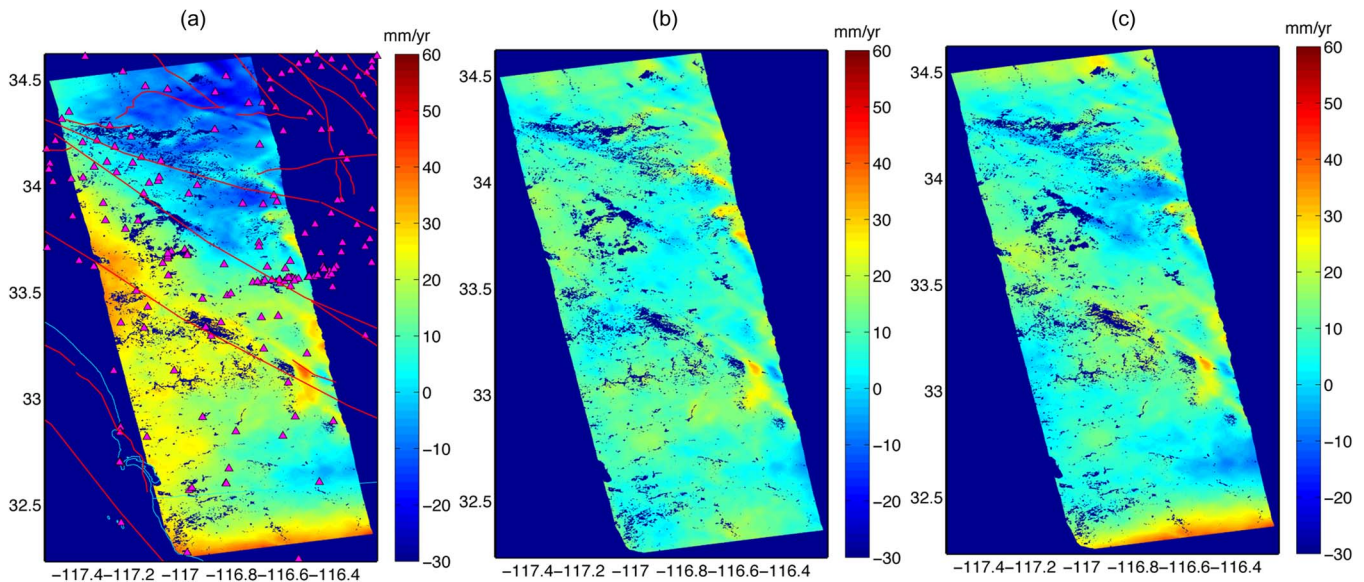


Fig. 6. InSAR LOS velocities obtained from the stacking of (a) original interferograms; (b) jointly corrected interferograms after correcting MAI-based ionosphere phase estimation and orbital ramp error; and (c) orbit-corrected interferograms using orbital phase estimation from 2-D polynomial fitting. Triangles in (a) indicate GPS locations from SCEC CMM-4. Only GPS sites within the InSAR image are used to compare with InSAR LOS measurements. Red lines are active fault traces from California Geological Survey fault database.

IV. DISCUSSIONS AND CONCLUSION

One of the main limitations in our joint correction of ionospheric and orbital artifacts is its requirement for good coherence for both InSAR and MAI interferograms. For southern California, due to its metropolitan setting and dry climate, the coherence is typically high even for the interferograms with temporal separation of more than 3 years [22]. Estimation of the ionospheric phase map from along-track MAI phase also requires the azimuth displacement due to ground deformation is negligible. For the ALOS ascending track used in this paper, we estimate the maximum azimuth displacement due to plate motion over a span of ~ 2 years is less than 7 cm. This is significantly less than the azimuth contribution (~ 1.3 m) caused by the ionospheric phase distortion. It is also well below the achieved accuracy of the MAI, which is about 0.8% of the azimuth resolution for ALOS PALSAR [11], equivalent to ~ 50 cm in our case.

Although the 2-D polynomial fit to original interferograms removes a considerable amount of long-wavelength orbital and ionospheric phase artifacts, this approach is not preferred, in particular, for interseismic deformation mapping because ionospheric artifacts cannot be simply modeled by a polynomial function. It is worthy to emphasize that the proposed joint

correction provides an effective way to correct both orbit- and ionosphere-related phase distortions. The method can be used with other methods to correct major noise sources in L-band SAR interferometry. It also lends itself naturally as a stand-alone correction module to correct orbital ramp error and ionosphere phase noise in L-band InSAR time-series analysis, which we do not address in this paper. For InSAR time-series analysis, the remaining atmospheric phase delay can be further suppressed by temporal filtering.

In this paper, we present an approach of joint correction of ionospheric phase artifacts and orbital ramp errors in InSAR imagery using MAI interferogram and *in situ* GPS measurements. Application of this approach to the selected examples of L-band InSAR images of interseismic deformation in southern California shows it can effectively correct the ionosphere related phase distortion and orbital ramp error. Remaining tropospheric phase delay can be further reduced through the stacking. We show that this systematic treatment of major noise sources in L-band InSAR measurements are critical for accurate measurement of interseismic deformation and need to be incorporated for continental scale deformation mapping for existing and future L-band SAR missions.

ACKNOWLEDGMENT

The authors would like to thank the GEO Supersites and the U.S. Government Research Consortium Datapool at the Alaska Satellite Facility for providing the ALOS PALSAR data, which are copyrighted Japan Aerospace Exploration Agency/Japanese Ministry of Economy, Trade and Industry.

REFERENCES

- [1] P. A. Rosen, S. Hensley, I. R. Joughin, F. K. Li, S. N. Madsen, E. Rodriguez, and R. M. Goldstein, "Synthetic aperture radar interferometry," *Proc. IEEE*, vol. 88, no. 3, pp. 333–382, Mar. 2000.
- [2] L. Zhang, Z. Lu, X. Ding, H.-S. Jung, G. Feng, and C.-W. Lee, "Mapping ground surface deformation using temporarily coherent point SAR interferometry: Application to Los Angeles Basin," *Remote Sens. Environ.*, vol. 117, pp. 429–439, Feb. 2012.
- [3] C. Zhao, Z. Lu, and Q. Zhang, "Time-series deformation monitoring over mining regions with SAR intensity-based offset measurements," *Remote Sens. Lett.*, vol. 4, no. 5, pp. 436–445, May 2013.
- [4] F. Meyer, R. Bamler, N. Jakowski, and T. Fritz, "The potential of low-frequency SAR systems for mapping ionospheric TEC distributions," *IEEE Geosci. Remote Sens. Lett.*, vol. 3, no. 4, pp. 560–564, Oct. 2006.
- [5] D. Raucoules and M. de Michele, "Assessing ionospheric influence on L-band SAR data: Implications on coseismic displacement measurements of the 2008 Sichuan earthquake," *IEEE Geosci. Remote Sens. Lett.*, vol. 7, no. 2, pp. 286–290, Apr. 2010.
- [6] F. Meyer, "A review of ionospheric effects in low-frequency SAR—Signals, correction methods, and performance requirements," in *Proc. IGARSS*, Jul. 2010, pp. 29–32.
- [7] F. Meyer and J. B. Nicoll, "Prediction, detection, and correction of Faraday rotation in full-polarimetric L-band SAR data," *IEEE Trans. Geosci. Remote Sens.*, vol. 46, no. 10, pp. 3076–3086, Oct. 2008.
- [8] R. Brcic, A. Parizzi, M. Eineder, R. Bamler, and F. Meyer, "Estimation and compensation of ionospheric delay for SAR interferometry," in *Proc. IGARSS*, Jul. 2010, pp. 2908–2911.
- [9] R. Brcic, A. Parizzi, M. Eineder, R. Bamler, and F. Meyer, "Ionospheric effects in SAR interferometry: An analysis and comparison of methods for their estimation," in *Proc. IGARSS*, Vancouver, BC, Canada, 2011, pp. 1497–1500.
- [10] P. Rosen, M. Lavalle, X. Pi, S. Buckley, W. Szeliga, H. Zebker, and E. Gurrola, "Techniques and tools for estimating ionospheric effects in interferometric and polarimetric SAR data," in *Proc. IGARSS*, Jul. 2011, pp. 1501–1504.
- [11] H.-S. Jung, D.-T. Lee, Z. Lu, and J.-S. Won, "Ionospheric correction of SAR interferograms by multiple-aperture interferometry," *IEEE Trans. Geosci. Remote Sens.*, vol. 51, no. 5, pp. 3191–3199, May 2013.
- [12] H.-S. Jung, J.-S. Won, and S.-W. Kim, "An improvement of the performance of multiple-aperture SAR interferometry (MAI)," *IEEE Trans. Geosci. Remote Sens.*, vol. 47, no. 8, pp. 2859–2869, Aug. 2009.
- [13] H.-S. Jung, Z. Lu, J. S. Won, M. P. Poland, and A. Miklius, "Mapping three-dimensional surface deformation by combining multiple-aperture interferometry and conventional interferometry: Application to the June 2007 eruption of Kilauea volcano, Hawaii," *IEEE Geosci. Remote Sens. Lett.*, vol. 8, no. 1, pp. 34–38, Jan. 2011.
- [14] H.-S. Jung, Z. Lu, and L. Zhang, "Feasibility of along-track displacement measurement from Sentinel-1 interferometric wide-swath mode," *IEEE Trans. Geosci. Remote Sens.*, vol. 51, no. 1, pp. 573–578, Jan. 2013.
- [15] N. B. Bechor and H. A. Zebker, "Measuring two-dimensional movements using a single InSAR pair," *Geophys. Res. Lett.*, vol. 33, no. 16, p. L16311, Aug. 2006.
- [16] H.-S. Jung, J.-S. Won, M.-H. Kang, and Y.-W. Lee, "Detection and restoration of defective lines in the SPOT 4 SWIR band," *IEEE Trans. Image Process.*, vol. 19, no. 8, pp. 2143–2156, Aug. 2010.
- [17] P. A. Rosen, S. Hensley, and G. Peltzer, "Updated repeat orbit interferometry package released," *Eos Trans. AGU*, vol. 85, no. 5, p. 47, Feb. 2004.
- [18] R. M. Goldstein and C. L. Werner, "Radar interferogram filtering for geophysical applications," *Geophys. Res. Lett.*, vol. 25, no. 21, pp. 4035–4038, Nov. 1998.
- [19] Z. K. Shen, R. W. King, D. C. Agnew, M. Wang, T. A. Herring, D. Dong, and P. Fang, "A unified analysis of crustal motion in Southern California, 1970–2004: The SCEC crustal motion map," *J. Geophys. Res.*, vol. 116, no. B11, p. B11402, Nov. 2011.
- [20] G. Peltzer, F. Crampé, S. Hensley, and P. Rosen, "Transient strain accumulation and fault interaction in the Eastern California shear Zone," *Geology*, vol. 29, no. 11, pp. 975–978, 2001.
- [21] P. Berardino, R. Lanari, and E. Sansosti, "A new algorithm for surface deformation monitoring based on small baseline differential SAR interferograms," *IEEE Trans. Geosci. Remote Sens.*, vol. 40, no. 11, pp. 2375–2383, Nov. 2002.
- [22] Z. Liu and P. Lundgren, "InSAR time series analysis of crustal deformation in Southern California from 1992–2010," presented at the AGU Fall Meeting, Dec. 2010. [Online]. Available: <http://adsabs.harvard.edu/abs/2010AGUFM.G13A0667L>



Zhen Liu received the M.S. and Ph.D. degrees in geophysics and space physics from the University of California at Los Angeles, Los Angeles, CA, USA, in 1999 and 2003, respectively.

He is currently a Scientist with Solid Earth Group of the Science Division, Jet Propulsion Laboratory, California Institute of Technology, Pasadena, CA, USA. His current research interests include using interferometric synthetic aperture radar and GPS to image and constrain time variable plate boundary deformation, investigate earthquake and volcano source processes, and monitor subsidence associated with groundwater dynamics.



Hyung-Sup Jung (M'09) received the M.S. and Ph.D. degrees in geophysics and remote sensing from Yonsei University, Seoul, Korea, in 1998 and 2007, respectively.

He is currently an Associate Professor with the Department of Geoinformatics, The University of Seoul, Seoul. His primary research interests include developments of synthetic aperture radar (SAR), interferometric SAR (InSAR), multiple-aperture InSAR (MAI) and small baseline subset (SBAS) InSAR processors, and algorithms related to 3-D deformation mapping by combining MAI and InSAR and 2-D surface velocity estimation by combining MAI and along-track interferometry.



Zhong Lu (S'96–A'97–M'97–SM'07) received the M.S. degree from Peking University, Beijing, China, in 1992 and the Ph.D. degree from the University of Alaska Fairbanks, Fairbanks, AK, USA, in 1996.

He is a Physical Scientist with Cascades Volcano Observatory, United States Geological Survey (USGS), Vancouver, WA, USA. He is a Principal Investigator of projects funded by the National Aeronautics and Space Administration (NASA), European Space Agency, Japan Aerospace Exploration Agency, German Aerospace Agency, and USGS on the study of land surface deformation using satellite interferometric synthetic aperture radar (SAR) (InSAR) imagery. His research interests include technique developments of SAR, InSAR, and persistent scatterer InSAR processing and their applications on natural hazard monitoring and natural resource management. He has produced more than 40 lead-authored and 70 coauthored peer-reviewed journal articles and book chapters focused on InSAR techniques and applications.

Dr. Lu was a recipient of an American Society for Photogrammetry and Remote Sensing Award for Best Scientific Paper in Remote Sensing, NASA Group Achievement Award, NASA Certificate of Appreciation, Raytheon Distinguished Level Award for Excellence in Technology, Science Applications International Corporation Technical Fellow, and Jerald Cook Memorial Award. He is a Committee Member of the International User Team for Radarsat-C SAR Constellations, the GeoEarthscope InSAR User Working Group, the NASA's Alaska Satellite Facility UserWorking Group, and NASA Deformation, Ecosystem Structure, and Dynamics of Ice-radar (DES/DynI-R) Science Definition Team.